MATERIALS SCIENCE

10.1126/sciadv.1500533

Origami-inspired active graphene-based paper for programmable instant self-folding walking devices

Jiuke Mu,[1]* Chengyi Hou,[1]* Hongzhi Wang,[1†] Yaogang Li,[2] Qinghong Zhang,[2†] Meifang Zhu[1]

Origami-inspired active graphene-based paper with programmed gradients in vertical and lateral directions is developed to address many of the limitations of polymer active materials including slow response and violent operation methods. Specifically, we used function-designed graphene oxide as nanoscale building blocks to fabricate an all-graphene self-folding paper that has a single-component gradient structure. A functional device composed of this graphene paper can (i) adopt predesigned shapes, (ii) walk, and (iii) turn a corner. These processes can be remote-controlled by gentle light or heating. We believe that this self-folding material holds potential for a wide range of applications such as sensing, artificial muscles, and robotics.

INTRODUCTION

Origami, the ancient art of paper folding, has inspired the design of various self-folding structures and devices for modern applications including remote control robotics (*1*, *2*), microfluidic chemical analysis (*3*), tissue engineering (*4*), and artificial muscles (*5*). Self-folding structures are rapidly emerging at the frontier of scientific and technological innovation because of their capability to perform programmed folding/unfolding motions without being kinematically manipulated by external forces or moments (*6*).

Active materials that convert other forms of energy into mechanical work to enable folding and unfolding operations are required to build a self-folding structure (*7*, *8*). Previous research on active materials has mainly focused on polymers, including gels (*9*), liquid crystalline polymers (*10*), shape memory polymers (SMPs) (*11*), and conjugated polymers (*12*). The properties of these materials respond to environmental stimuli (pH, temperature, solvent, humidity, electricity, and light), which causes their shape to change (*13*). To date, three general mechanisms have been used to self-fold polymers: (i) relaxation of SMPs, (ii) folding of hybrid polymer bilayers with vertical inhomogeneity or patterned films with lateral inhomogeneity induced by the different deformation capability of each component, and (iii) folding of single-component planar polymers by applying field gradients to uniform structures or nongradient stimuli to gradient structures. Although these can be efficient approaches, they still face a number of practical challenges. Regarding approach (i), SMPs are limited by the number of temporary shapes that can be memorized in each shape memory cycle and the ability to tune the shape memory transition temperature(s) for target applications (*14*). Considering approach (ii), a disadvantage of polymer multilayers is their poor stability. The multiple components do not uniformly expand/shrink, which causes interface problems. This approach also typically requires wires and circuit connections (*15*, *16*), which are not suitable for remote applications. Meanwhile, for approach (iii), both the fabrication of gradient polymer films and the generation of gradient stimulus fields are complicated, even though this is a general strategy to obtain self-folding single-component polymers. It is also difficult to use this kind of self-folding polymer to produce structures that move or turn. In addition, such structures usually operate under nonphysiological conditions [for example, temperature >100°C (*17*), organic vapor, dangerous voltage (*15*), chemical reaction (*18*), and acid/alkaline solution (*19*)], and in other cases, their actuations are slow, ranging from a few tens of seconds (*20*) to several minutes (*21*), or are even irreversible (*22*).

Although they have value in a certain context, the existing origami-inspired designs do not yet meet the requirements for practical use. It is therefore of fundamental and practical significance to explore alternative approaches to realize self-folding structures. Very recently, origami-inspired graphene nanocages were predicted (*23*), revealing the promise of graphene as a material to obtain self-folding machines or robots. Graphene can be considered as a two-dimensional (2D) active polymer (*24*) but is much stronger and more versatile than traditional polymers (*25*). To meet the operating conditions for self-folding devices and other application requirements, one has to translate the active properties of individual graphene sheets to the macroscale. Encouragingly, graphene nanosheets have been used as nanoscale building blocks to construct various kinds of 3D assemblies (*26*, *27*). Stimuli-responsive hydrogel-, paper-, and fiber-like macroscopic graphene materials (MGMs) are readily available (*28*, *29*). MGMs very strongly absorb light over a broad range extending from ultraviolet to infrared (IR) wavelengths, which should facilitate the use of light energy to accomplish photomechanical work conversion. Because of the strong π-π interactions between graphene layers, MGMs contain no unstable interfaces; hence, they can be superelastic and flexible as well as mechanically strong (*26*). However, to date, programmed self-folding and motions of graphene at the macroscale are still difficult to achieve. In other words, although it has been considered, macroscale graphene origami is largely unexplored.

Here, an instant self-folding graphene paper with a programmed dual-gradient (vertical and lateral) structure is developed to address many of the issues facing self-folding structures described above. That is, we use function-designed graphene oxide (GO) nanoscale building blocks to fabricate a self-folding all-graphene paper that represents both a single-component gradient structure and a functional device that demonstrates three capabilities: (i) producing predesigned shapes, (ii) walking, and (iii) turning a corner. The performance of this paper can be remote-controlled by exposure to gentle light or heat.

[1]State Key Laboratory for Modification of Chemical Fibers and Polymer Materials, College of Materials Science and Engineering, Donghua University, Shanghai 201620, People's Republic of China. [2]Engineering Research Center of Advanced Glasses Manufacturing Technology, Ministry of Education, Donghua University, Shanghai 201620, People's Republic of China.
*These authors contributed equally to this work.
†Corresponding author. E-mail: wanghz@dhu.edu.cn (H.W.); zhangqh@dhu.edu.cn (Q.Z.)

RESULTS

Fabrication and characterization of self-folding graphene paper

Paper-like MGMs with vertical and lateral dual gradients (fig. S1) were fabricated by filtering GO and GO–polydopamine (PDA) solutions. Pure GO solution was synthesized according to the modified Hummers method (*30*). GO-PDA solution was produced by the self-polymerization of a GO–dopamine (DA) mixture (see Fig. 1A and Materials and Methods). Atomic force microscope (AFM) images showed that after polymerization of DA, PDA aggregated on the surface of GO. The thickness of monolayer GO-PDA increased from 1.5 to about 5 nm. DA is usually used to reduce GO to form reduced GO (rGO) (*31*). However, here, we found that a certain amount of DA polymerized on a GO nanosheet could protect GO from chemical reduction. After a mask-assisted filtration process (see Fig. 1B and Materials and Methods), the obtained dual-gradient GO paper was reduced by hydriodic acid (HI) and thoroughly washed under ambient laboratory conditions (*32*). Because of the protection provided by PDA, the GO region covered by a polycarbonate (PC) mask remained hydrophilic with a contact angle (CA) of about 43.1°, whereas the other regions became hydrophobic (CA = 93.4°) and changed from black to a shiny metallic luster. X-ray photoelectron spectra (XPS) of the mask region showed a strong peak at 285.2 eV that was attributed to C–N bonding, indicating the grafting of PDA on the GO sheets (fig. S2). The C/O ratio was only 3.62, indicating that the GO in the GO-PDA region was not reduced. In contrast, without PDA protection, the GO in other regions was efficiently reduced to form rGO, and the C/O ratio increased to 7.81. X-ray diffraction (XRD) patterns and Raman spectra were consistent with the above results (see figs. S3 and S4, respectively).

The PDA grafted on the GO nanosheet not only protected it from reduction but also formed cross-links between the GO nanosheets in both the GO-PDA regions and the interface between rGO and GO-PDA regions (*31*). As a result, GO-PDA was in close contact with

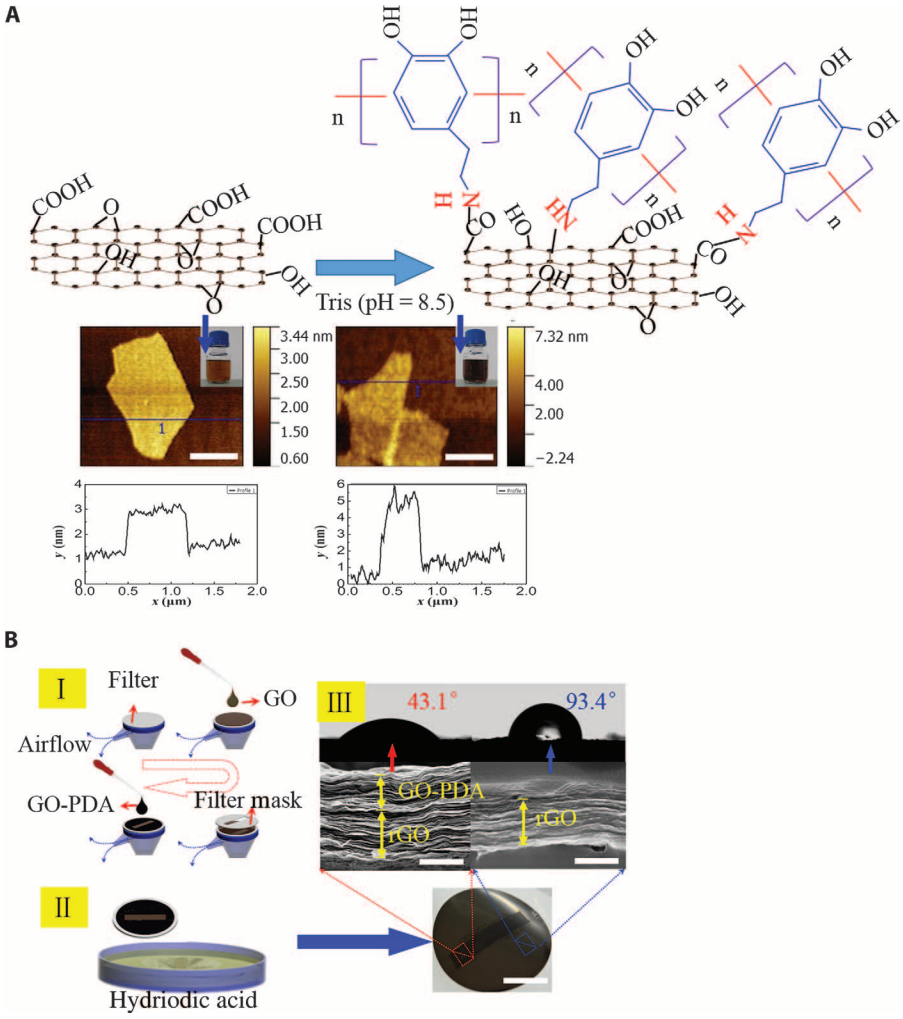

Fig. 1. Fabrication and characterization of the MGM paper. (**A**) Schematic illustration of the synthesis of GO-PDA. The AFM image and height profile of GO (left) and GO-PDA (right) spin-coated on a silicon wafer (scale bar, 1 μm). (**B**) (I) Schematic illustration of the mask-assisted filtration process (scale bar, 2 cm). (II) Cross-sectional SEM images of GO-PDA/rGO and rGO regions after reduction by HI (scale bar, 1 μm). (III) CA measurement of the GO-PDA/rGO surface (43.1°) and rGO surface (93.4°) of dual-gradient MGM.

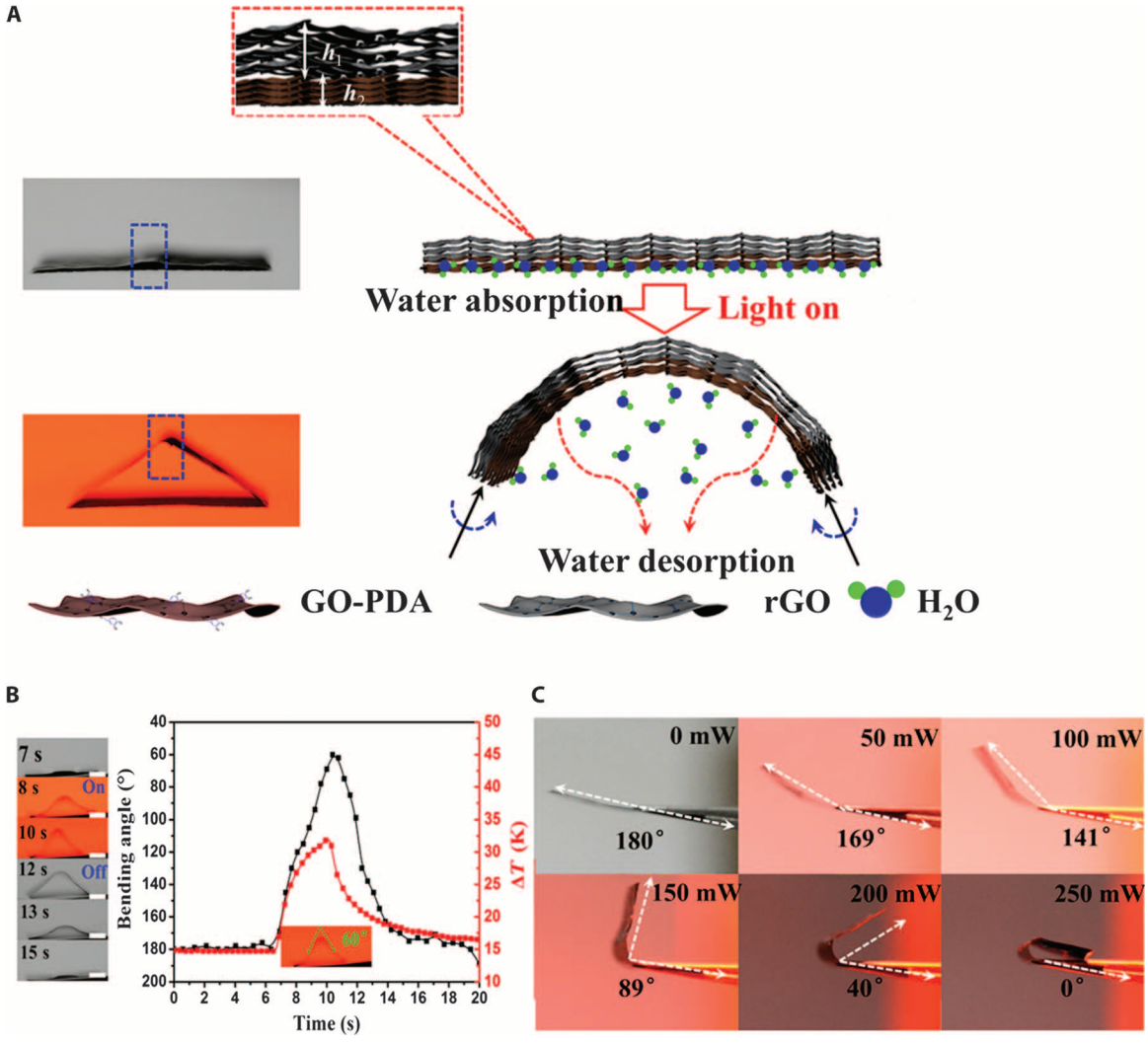

Fig. 2. GO-PDA/rGO photoactuators and photothermal actuation mechanism. (**A**) Schematic representations of the structures and mechanisms of the graphene paper. If there is no NIR light irradiation, the GO-PDA/rGO region flattens. A flat, freestanding GO-PDA/rGO region starts to bend immediately upon exposure to NIR light irradiation. This bending/unbending mechanism is completely reversible over many cycles. (**B**) Series of optical images showing the light actuation process of the MGM (100 mW cm^{-2}) (scale bar, 3 mm). Bending angle as a function of time as light is turned on (period, 8 s) and off (period, 12 s). (**C**) Dependence of bending angle on illumination intensity (scale bar, 5 mm).

the underlying rGO, as shown in the scanning electron microscopy (SEM) images in Fig. 1B and fig. S5. The cross-linking effect of PDA increases the gravimetric tensile strength of the integrated GO-PDA/rGO paper compared with the rGO paper (fig. S6). These results indicate that the graphene paper produced here was mechanically strong and stable.

Self-folding mechanism of the dual-gradient graphene paper

In the dual-gradient MGM, the GO-PDA region could readily adsorb/desorb water molecules in response to environmental humidity, temperature, or light, which resulted in swelling/shrinking of the GO sheets (*33*). In contrast, the rGO was inert to water molecules. Considering this behavior together with the excellent photothermal properties of rGO and GO (*34*), as well as its high flexibility and mechanical robustness, this graphene paper holds great potential for photoresponsive actuator applications. Figure 2A illustrates the actuation mechanism of the graphene paper, which matches well with experimental observations. The bending/unbending of the MGM was induced by the different water absorption/desorption abilities of GO-PDA and rGO. The GO-PDA regions composed of hydrophilic PDA and GO sheets had great ability to absorb/desorb water as the temperature was increased/decreased. In contrast, the hydrophobic RGO regions were inert to temperature changes. The difference in absorption/desorption abilities led to a mismatch in the expansion/contraction of GO-PDA and rGO regions during a change in environmental temperature. As a result of which, the volume of the GO-PDA region changed (fig. S7, A and B) and interfacial stress was generated to induce bending/unbending of the MGM (Fig. 2A). The time-dependent weight changes of the MGM under on/off irradiation and the attenuated total reflectance (ATR)–IR spectra (fig. S7, C and D) could be further verifications of this mechanism. Figure 2B shows that the paper was also highly sensitive to light. A flat, freestanding MGM started to bend immediately upon irradiation with

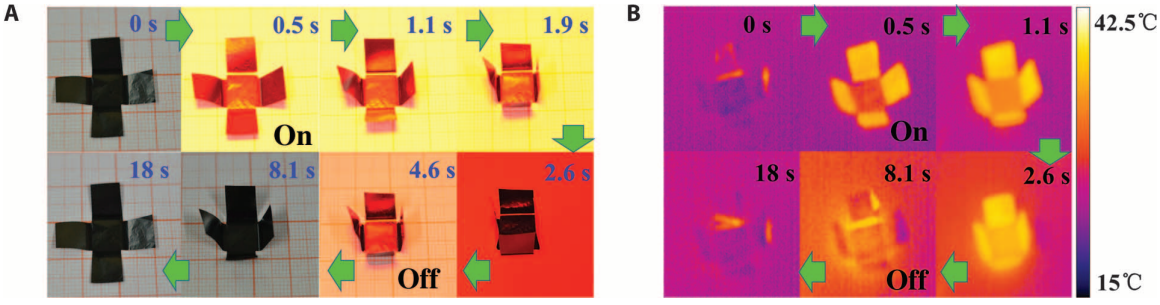

Fig. 3. A fast self-folding box driven by light. (**A**) Time profiles of self-folding movements of a cross-shaped piece of paper with and without NIR light irradiation. The sample was placed on the platform and illuminated with NIR light (100 mW cm^{-2}) normal to its surface (light is incident from above). (**B**) IR images of the self-folding box with and without light illumination (100 mW cm^{-2}, NIR light).

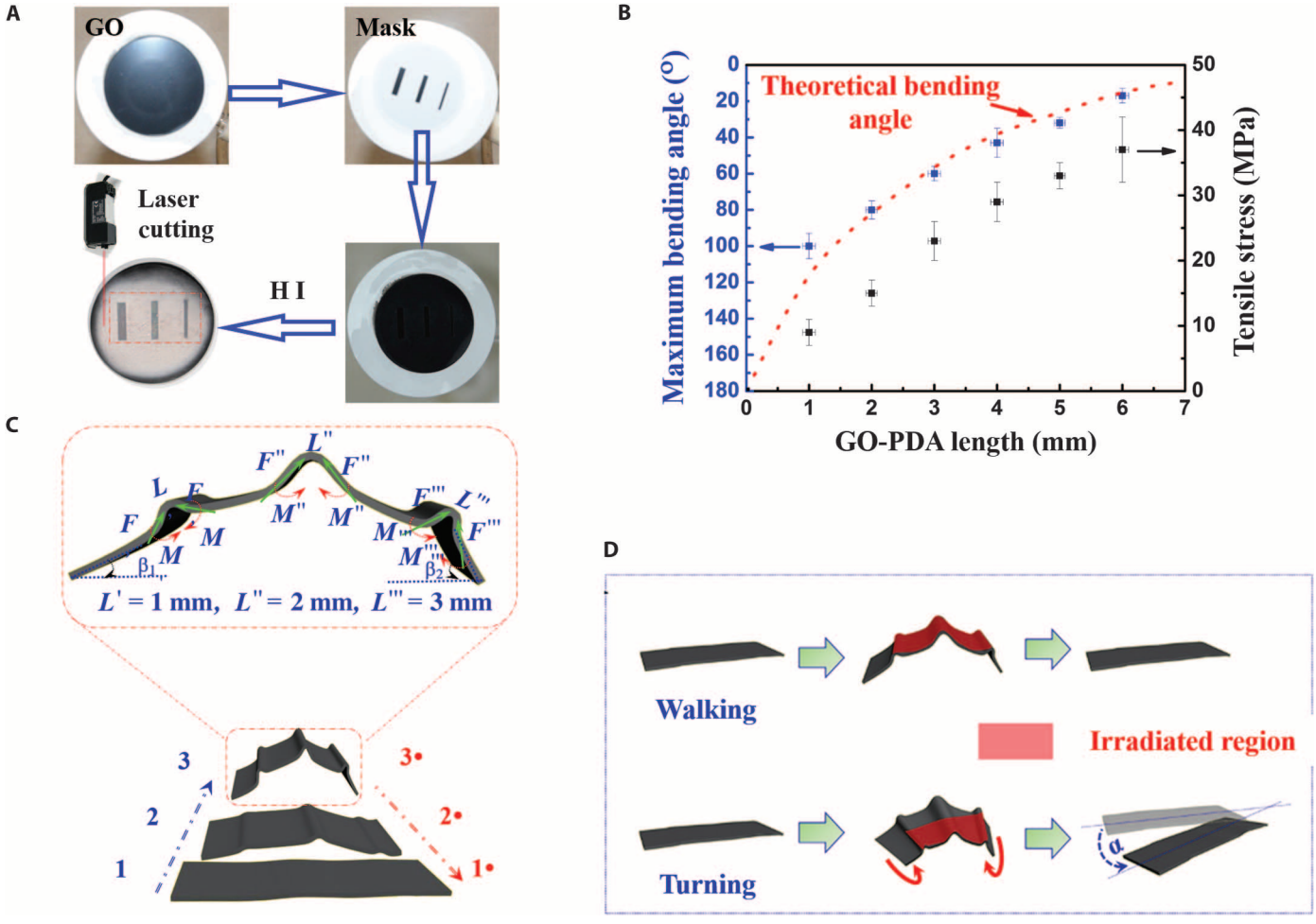

Fig. 4. The walking and turning mechanism of the wormlike walking device. (**A**) Scheme outlining fabrication of the walking device. (**B**) Maximum output stress (black spots), bending angle (blue spots), and theoretical bending angle (dotted red line) as a function of GO-PDA width. (**C**) Illustrations of the walking movements of the device, and the mechanical model used to describe the walking behavior (L', L'', and L''' are the width of three different GO-PDA lines; F', F'', and F''' are the stress generated by three different GO-PDA lines; M', M'', and M''' denote the bending moment about the central axis. β_1 and β_2 are the angles between MGM and the horizontal plane). (**D**) Model used to describe turning behavior controlled by light.

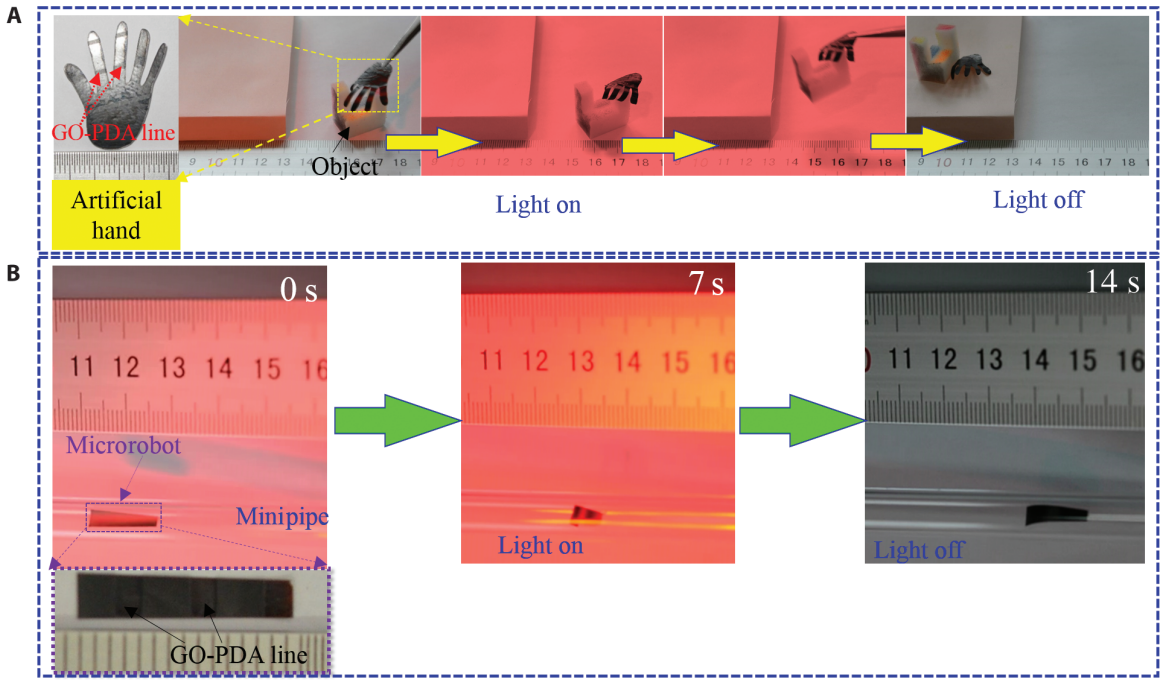

Fig. 5. The demonstration of the hand and wormlike auto device completing various bending and stretching actions. (**A**) Optical images showing artificial/robotic hand holding an object driven by light irradiation. (**B**) Optical images showing the "microrobot" crawling progressing in the pipeline driven by light irradiation.

near-IR (NIR) light, bending to nearly 60° within 2 s. After switching off the light, the film recovered to its original shape within 3 s at 40% relative humidity. It was also found that the recovery speed increased with increasing relative humidity (as shown in fig. S8). The bending angles (θ) and changes in temperature of the paper during this process were recorded. The two curves fitted very well, which confirmed that the bending is initiated by photoinduced heat. Some properties (microstructure and macroperformance) of the graphene paper are able to undergo a transition, but unlike most polymers, there is no critical transition condition, which makes them much easier to operate. Figure 2C and fig. S9 show θ of the graphene paper as a function of light intensity. Irradiating the paper for 2 s using NIR light with intensities of 50, 100, 150, 200, and 250 mW cm^{-2} resulted in θ of 169°, 141°, 89°, 40°, and 0°, respectively.

The actuation behavior of the graphene paper is programmable. A self-folding box was made from the graphene paper (as shown in fig. S10). As illustrated in Fig. 3A and movie S1, a cross-shaped piece of graphene paper folded itself into a box in 200 ms under NIR light. Then, when the NIR light was turned off, the box unfolded back into its original cross shape. To elucidate the underlying photothermally driven mechanism of self-folding, we used an IR camera to measure the real-time temperature changes of the paper upon light irradiation. Figure 3B depicts the temperature profile of the self-folding box when the light is on and off, which confirms that the self-folding behavior is initiated by the photoinduced heat.

Walking mechanism of graphene paper

We explored the relationship between θ and the final output stress (F_0) of the bilayer structure depending on the width of the GO-PDA layers. A series of GO-PDA lines of different width (L) were patterned on rGO films using our approach (Fig. 4A). The generated stress of these MGMs was measured using a universal testing machine (*35*). Samples were cut into the same size (8 × 10 mm), clamped, and preloaded with a stress of 0.01 MPa to keep them tight and straight. An NIR light (250 mW cm^{-2}) was used to irradiate the MGMs. Figure 4B shows that the stress generated by the MGM (with 6-mm GO-PDA lines) exceeds 44 MPa after deducing the prestress (figs. S11 and S12). This is almost two orders of magnitude higher than that of mammalian skeletal muscle (0.35 MPa) (*36*). Upon laser irradiation (200 mW cm^{-2}), an MGM with a 3-mm GO-PDA line (1 mg) can deform and lift a 120-mg load (titanium foil) by 7 mm within 3.2 s (fig. S13). The maximum energy conversion efficiency during contraction was 1.8% (see note S1). This actuator efficency is comparable to those of polymer muscle and commercial shape memory metals (*17*). The power density was calculated to be 2.6 W kg^{-1} (see note S1), which is comparable to that of a reported moisture-triggered polymer actuator (2.5 W kg^{-1}) (*36*). The reliability and stability of its performance were further examined by applying on/off NIR light. The sample retained 90% of its output stress capacity after 500 cycles (fig. S14).

The stresses generated by the GO-PDA lines increased with L, exhibiting an approximately linear relationship (Fig. 4B, fig. S11, and table S1). Both L and F_0 can be fitted with an exponential response using Eq. 1

$$F_0 = kL \quad (1)$$

where k is the scale factor. Beam theory was used to further explain the bending/folding process and identify the governing parameters. The rGO and GO-PDA regions can be thought of as two separate layers with uniform thicknesses of h_1 and h_2, respectively (Fig. 2A). For simplicity, we assumed that the MGM actuator was not prebent; that is, there was no stress in the

actuator before irradiation. Exposure to NIR light led to convex upward bending of the paper. The curvature 1/ρ of the paper can be fitted with an exponential response according to Eq. 2 (*13*)

$$1/\rho = 6F_0(h_1 + h_2)/(E_1{h_1}^3 + E_2{h_2}^3) \quad (2)$$

where E_1 and E_2 are Young's moduli of the GO-PDA and rGO regions, respectively. Combining Eqs. 1 and 2 gives

$$1/\rho = 6kL(h_1 + h_2)/(E_1{h_1}^3 + E_2{h_2}^3) \quad (3)$$

In addition, we deduced the following equation according to the definition of curvature radius (ρ)

$$1/\rho = [\pi(180 - \theta)]/180L \quad (4)$$

Combining Eqs. 3 and 4 gives

$$\theta = 180 - [1080kL^2(h_1 + h_2)]/[\pi(E_1{h_1}^3 + E_2{h_2}^3)] \quad (5)$$

Equation 5 reveals that the bending angle of MGMs can be controlled by changing the width of the GO-PDA lines. In this case, the photoresponsive bending/unbending of the GO-PDA/rGO actuators allowed us to produce materials that are capable of self-folding into desired 3D structures. We also constructed a light-driven walking device by patterning a series of GO-PDA lines of different size on a rGO film (Fig. 4A).

Figure 4C depicts the walking of the device on a substrate. The walking behavior occurs in five sequential steps (1→2→3→2•→1•) that are controlled by NIR light. Initially, the whole device bent upward into an arch because the GO-PDA layer was swollen at low temperature. The GO-PDA layer then contracted upon laser irradiation, which caused the walking device to stretch forward along the direction of the narrower GO-PDA line (1→2→3). When the laser was turned off, the GO-PDA layer became swollen again and the device bent into an arch (3→2•→1•) (fig. S15). By switching the laser on and off, the device unidirectionally walked in a step-by-step manner driven by the interfacial stress between the GO-PDA and rGO layers (movies S2 and S3). Surprisingly, one walking cycle (five steps) of the device took only 2 s because of the strong water adsorption/desorption ability of GO-PDA and the high photothermal conversion efficiency of rGO. Figure 4D reveals that the walking devices not only can exhibit forward motion but also can turn when exposed to an IR laser. Theoretical analysis of the turning mechanism is illustrated in fig. S15. Irradiating one side of the film by an IR laser resulted in asymmetric bending. Such asymmetric bending of the bilayer actuator in the walking device was induced by the uneven distribution of temperature at its surface (fig. S16). We can see that the distribution of the active region is so flexible that the bending behavior occurred only on the irradiated side whereas the other side remained flat (see Fig. 4D, fig. S16, and movie S4). When the laser light was turned off, the GO-PDA layer absorbed water from the environment and became swollen again. In this way, the device turned by a certain angle (α). Upon periodic exposure to laser light, various α were achieved (fig. S17). Unlike previously reported walking devices by Ma *et al.* (*13*), our walking devices can turn and exhibit forward and backward motion driven by an IR laser. A demonstration of the self-folding device completing various walking and turning actions is shown in fig. S18. In addition, we have also shown that it has promising potential to serve as an artificial hand (grasping and holding objects five times heavier than itself, as shown in Fig. 5A and movie S5) or a microrobot (remotely operating inside a sealed and minispace barely reached by mechanical force and electricity, as shown in Fig. 5B and movie S6). This whole process was completed under IR laser control without using any other external stress.

DISCUSSION

We fabricated an all-carbon light-driven walking device that can change direction and other kinds of smart devices capable of performing well-designed motions by patterning an action layer of GO-PDA lines on a supporting layer of rGO by a facile, low-cost process at room temperature. The GO-PDA layer can absorb water from the environment, causing it to swell and lose water upon NIR/laser light irradiation and thus inducing shrinkage. As a supporting layer, the high photothermal conversion efficiency and fluffy structure of the rGO film played an important role in transferring humidity-responsive GO-PDA into light-driven actuators with fast response, excellent light sensitivity, large deflection angle, and reversibility. We believe that these devices have the potential to be adapted to a wide range of applications such as sensing, artificial muscles, and robotics. The present study also provided a practical method for future large-scale preparation of self-folding devices using an approach similar to printing.

MATERIALS AND METHODS

Synthesis of GO-PDA nanocomposites

All reagents were of analytical grade and used as obtained without further purification. GO was synthesized by the modified Hummers method (*27*). PDA-functionalized graphene nanosheets (GO-PDA nanocomposites) were prepared by the following procedure using DA as a surface functionalization agent. An aqueous solution of GO (15 ml, 1 mg ml^{-1}) and DA hydrochloride (0.013 mg ml^{-1}) were mixed to form a uniform solution after sonication for 100 min. The pH value of the mixed solution was buffered close to 8.5 using tris-Cl ($C_4H_{11}NO_3$) solution. The reaction mixture was stirred at 45°C for 12 hours. Then, the GO-PDA nanocomposites were obtained after purifying by centrifugation and washing.

Fabrication of a rGO/GO-PDA self-folding film

An aqueous solution of GO (50 ml, 1 mg ml^{-1}) was formed after sonication for 100 min. Vacuum filtration was performed using a standard setup with a PC membrane (Daojin, 0.22-μm pore size, 25-mm diameter). After filtration, the wet GO film was covered with a PC mask (50 cm in diameter). GO-PDA solution (15 ml) was added on top of the PC mask and then subjected to vacuum filtration. The composite films were subsequently peeled off the PC membrane and immersed in 55% HI solution at room temperature for 1 hour. The resulting rGO/GO-PDA film was washed with deionized water several times.

Characterization and measurements

The morphologies of the as-prepared samples were determined by SEM (JSM-6700F, JEOL), and samples were embedded in epoxy resin before imaging. Photographs were taken using a single-lens reflex camera (D7000, Nikon). XPS measurements were performed using a Kratos AXIS ULTRA Multifunctional X-ray Photoelectron Spectroscope, and the typical detection depth is ~5 nm. All XPS spectra were corrected using the C 1s line at 284.6 eV. CA measurements were conducted

using a CA meter (OCA40, Dataphysics) at ambient temperature. Deionized water (5 μl) was dropped onto each sample using an automatic dispenser, and the CA of each droplet was automatically determined using the Laplace-Young fitting algorithm. The electrical conductivity of the paper samples was measured using the four-point probe method (MCP-360, Mitsubishi Chemical Analytech Co. Ltd.). AFM images were recorded using an AFM (Nanoscope IV SPM, Digital Instruments). A laboratory balance (AL204, Mettler Toledo) was used to collect mass data. Temperatures and IR thermal images were recorded using an IR thermometer (FLIR A40M, ThermoVision). The bending angle was measured using a laser displacement sensor (see fig. S19). ATR-IR spectra were recorded on a Nicolet NEXUS 670 spectrometer. The stress generated by the graphene actuator and its strength were measured on a universal testing machine (Instron Model 5969, Instron). An IR light source (250 W max, Philips BR125) was used in Figs. 2 to 5 and figs. S7, S8, S9, S11, S13, S14, and S19. Another Vis-NIR light source (400 to 1100 nm, 20 W max, SFOLT Co. Ltd.) was used to irradiate the actuator in figs. S12, S15, S16, S17, and S18.

SUPPLEMENTARY MATERIALS

Supplementary material for this article is available at http://advances.sciencemag.org/cgi/content/full/1/10/e1500533/DC1

Fig. S1. Schematic illustration of the MGM having a dual-gradient structure with vertical and lateral gradients.

Fig. S2. The XPS survey spectra of GO-PDA/HI and rGO.

Fig. S3. Powder XRD patterns of GO, GO-PDA, GO-PDA/HI, rGO, and graphite.

Fig. S4. Raman spectra of GO, GO-PDA, GO-PDA/HI, and rGO.

Fig. S5. Optical images show the adhesive tape–peeling method (top).

Fig. S6. The gravimetric tensile strength of GO-PDA/rGO and rGO regions.

Fig. S7. The thickness profiles of the GO-PDA line with light on and off.

Fig. S8. The digital photograph of the moisture control device and the recovery performance tested at different relative humidity environments.

Fig. S9. Schematic illustration of θ, γ, *L*, *F*, and ρ (*L* is the width of the GO-PDA line; *F* is the stress generated by the GO-PDA line; ρ is the radius of curvature; θ is the bending angle of MGM; γ is the supplementary angles of θ).

Fig. S10. Schematic illustration of the preparation of a self-folding box.

Fig. S11. The stress generated by the MGMs (**middle** and **right**) were measured on the universal testing machine (Instron Model 5969) with on/off NIR light irradiations (**left**).

Fig. S12. Cross-sectional field emission SEM images indicating GO-PDA/rGO regions for different GO-PDA lines: (**A**) 1 mm, (**B**) 3 mm, and (**C**) 5 mm.

Fig. S13. Temperature-change curves and the energy conversion efficiency of MGM.

Fig. S14. Cycle output test of MGM under on/off irradiations.

Fig. S15. Optical image of the walking behavior of the walking device driven by NIR light.

Fig. S16. The turning behavior of the walking device.

Fig. S17. Turning angle of the walking devices as a function of time as light is turned on and off for different illumination areas.

Fig. S18. Optical images show the walking device progressing over a virtual map driven by light irradiation (scale bar, 3 cm).

Fig. S19. The schematic illustration and optical image showing the measurement of the bending angle using a laser displacement sensor.

Table S1. Maximum output stress, bending angle, and theoretical bending angle as a function of GO-PDA width (average value of data).

Note S1. Calculations of the maximum energy conversion efficiency of our actuator.

Methods

Movie S1. The photoactuation behavior of the self-folding box.

Movie S2. The walking behavior of the wormlike walking device driven by an NIR light on and off (100 mW cm^{-2}).

Movie S3. The worming behavior of the wormlike walking device driven by an NIR light on and off (100 mW cm^{-2}).

Movie S4. The turning behavior of the wormlike walking device driven by an IR laser.

Movie S5. The grasping behavior of the "artificial/robotic hand" driven by light irradiation.

Movie S6. The crawling behavior of the "microrobot" inside a minipipe driven by an NIR light on and off (100 mW cm^{-2}).

REFERENCES AND NOTES

1. S. Felton, M. Tolley, E. Demaine, D. Rus, R. Wood, A method for building self-folding machines. *Science* **345**, 644–646 (2014).
2. E. Hawkes, B. An, N. M. Benbernou, H. Tanaka, S. Kim, E. D. Demaine, D. Rus, R. J. Wood, Programmable matter by folding. *Proc. Natl. Acad. Sci. U.S.A.* **107**, 12441–12445 (2010).
3. H. Liu, R. M. Crooks, Three-dimensional paper microfluidic devices assembled using the principles of origami. *J. Am. Chem. Soc.* **133**, 17564–17566 (2011).
4. P. A. Troshin, D. K. Susarova, Y. L. Moskvin, I. E. Kuznetsov, S. A. Ponomarenko, E. N. Myshkovskaya, K. A. Zakharcheva, A. A. Balakai, S. D. Babenko, V. F. Razumov, Impedance measurements as a simple tool to control the quality of conjugated polymers designed for photovoltaic applications. *Adv. Funct. Mater.* **20**, 4351–4357 (2010).
5. H. Stoyanov, M. Kollosche, S. Risse, R. Waché, G. Kofod, Soft conductive elastomer materials for stretchable electronics and voltage controlled artificial muscles. *Adv. Mater.* **25**, 578–583 (2013).
6. J. L. Silverberg, A. A. Evans, L. McLeod, R. C. Hayward, T. Hull, C. D. Santangelo, I. Cohen, Using origami design principles to fold reprogrammable mechanical metamaterials. *Science* **345**, 647–650 (2014).
7. X. Li, M. J. Serpe, Understanding and controlling the self-folding behavior of poly(*N*-isopropylacrylamide) microgel-based devices. *Adv. Funct. Mater.* **24**, 4119–4126 (2014).
8. M. Jamal, A. M. Zarafshar, D. H. Gracias, Differentially photo-crosslinked polymers enable self-assembling microfluidics. *Nat. Commun.* **2**, 527 (2011).
9. A. Sidorenko, T. Krupenkin, A. Taylor, P. Fratzl, J. Aizenberg, Reversible switching of hydrogel-actuated nanostructures into complex micropatterns. *Science* **315**, 487–490 (2007).
10. W. Lu, A. G. Fadeev, B. Qi, E. Smela, B. R. Mattes, J. Ding, G. M. Spinks, J. Mazurkiewicz, D. Zhou, G. G. Wallace, D. R. MacFarlane, S. A. Forsyth, M. Forsyth, Use of ionic liquids for π-conjugated polymer electrochemical devices. *Science* **297**, 983–987 (2002).
11. A. Lendlein, S. Kelch, Shape-memory polymers. *Angew. Chem. Int. Ed. Engl.* **41**, 2034–2057 (2002).
12. E. Smela, Conjugated polymer actuators for biomedical applications. *Adv. Mater.* **15**, 481–494 (2003).
13. Y. Ma, Y. Zhang, B. Wu, W. Sun, Z. Li, J. Sun, Polyelectrolyte multilayer films for building energetic walking devices. *Angew. Chem. Int. Ed. Engl.* **123**, 6378–6381 (2011).
14. T. Xie, Tunable polymer multi-shape memory effect. *Nature* **464**, 267–270 (2010).
15. R. Pelrine, R. Kornbluh, Q. Pei, J. Joseph, High-speed electrically actuated elastomers with strain greater than 100%. *Science* **287**, 836–839 (2000).
16. R. H. Baughman, C. Cui, A. A. Zakhidov, Z. Iqbal, J. N. Barisci, G. M. Spinks, G. G. Wallace, A. Mazzoldi, D. De Rossi, A. G. Rinzler, O. Jaschinski, S. Roth, M. Kertesz, Carbon nanotube actuators. *Science* **284**, 1340–1344 (1999).
17. C. S. Haines, M. D. Lima, N. Li, G. M. Spinks, J. Foroughi, J. D. W. Madden, S. H. Kim, S. Fang, M. J. de Andrade, F. Göktepe, Ö. Göktepe, S. M. Mirvakili, S. Naficy, X. Lepró, J. Oh, M. E. Kozlov, S. J. Kim, X. Xu, B. J. Swedlove, G. G. Wallace, R. H. Baughman, Artificial muscles from fishing line and sewing thread. *Science* **343**, 868–872 (2014).
18. M. Nakahata, Y. Takashima, A. Hashidzume, A. Harada, Redox-generated mechanical motion of a supramolecular polymeric actuator based on host–guest interactions. *Angew. Chem. Int. Ed. Engl.* **52**, 5731–5735 (2013).
19. W. Guo, C.-H. Lu, R. Orbach, F. Wang, X.-J. Qi, A. Cecconello, D. Seliktar, I. Willner, pH-stimulated DNA hydrogels exhibiting shape-memory properties. *Adv. Mater.* **27**, 73–78 (2015).
20. Y. Zhang, Y. Ma, J. Sun, Reversible actuation of polyelectrolyte films: Expansion-induced mechanical force enables *cis-trans* isomerization of azobenzenes. *Langmuir* **29**, 14919–14925 (2013).
21. Y. Takashima, S. Hatanaka, M. Otsubo, M. Nakahata, T. Kakuta, A. Hashidzume, H. Yamaguchi, A. Harada, Expansion–contraction of photoresponsive artificial muscle regulated by host–guest interactions. *Nat. Commun.* **3**, 1270 (2012).
22. O. S. Bushuyev, A. Tomberg, T. Friščić, C. J. Barrett, Shaping crystals with light: Crystal-to-crystal isomerization and photomechanical effect in fluorinated azobenzenes. *J. Am. Chem. Soc.* **135**, 12556–12559 (2013).
23. L. Zhang, X. Zeng, X. Wang, Programmable hydrogenation of graphene for novel nanocages. *Sci. Rep.* **3**, 3162 (2013).
24. V. Palermo, Not a molecule, not a polymer, not a substrate… the many faces of graphene as a chemical platform. *Chem. Commun.* **49**, 2848–2857 (2013).
25. C. Lee, X. Wei, J. W. Kysar, J. Hone, Measurement of the elastic properties and intrinsic strength of monolayer graphene. *Science* **321**, 385–388 (2008).
26. L. Qiu, J. Z. Liu, S. L. Y. Chang, Y. Wu, D. Li, Biomimetic superelastic graphene-based cellular monoliths. *Nat. Commun.* **3**, 1241 (2012).
27. J. Shui, M. Wang, F. Du, L. Dai, N-doped carbon nanomaterials are durable catalysts for oxygen reduction reaction in acidic fuel cells. *Sci. Adv.* **1**, e1400129 (2015).
28. S. Park, J. An, J. W. Suk, R. S. Ruoff, Graphene-based actuators. *Small* **6**, 210–212 (2010).
29. H. Cheng, J. Liu, Y. Zhao, C. Hu, Z. Zhang, N. Chen, L. Jiang, L. Qu, Graphene fibers with predetermined deformation as moisture-triggered actuators and robots. *Angew. Chem. Int. Ed. Engl.* **52**, 10482–10486 (2013).

30. W. S. Hummers Jr., R. E. Offeman, Preparation of graphitic oxide. *J. Am. Chem. Soc.* **80**, 1339 (1958).
31. W. Cui, M. Li, J. Liu, B. Wang, C. Zhang, L. Jiang, Q. Cheng, A strong integrated strength and toughness artificial nacre based on dopamine cross-linked graphene oxide. *ACS Nano* **8**, 9511–9517 (2014).
32. C. Hou, H. Wang, Q. Zhang, Y. Li, M. Zhu, Highly conductive, flexible, and compressible all-graphene passive electronic skin for sensing human touch. *Adv. Mater.* **26**, 5018–5024 (2014).
33. X. Ma, M. R. Zachariah, C. D. Zangmeister, Crumpled nanopaper from graphene oxide. *Nano Lett.* **12**, 486–489 (2012).
34. A. A. Balandin, Thermal properties of graphene and nanostructured carbon materials. *Nat. Mater.* **10**, 569–581 (2011).
35. J. Mu, C. Hou, B. Zhu, H. Wang, Y. Li, Q. Zhang, A multi-responsive water-driven actuator with instant and powerful performance for versatile applications. *Sci. Rep.* **5**, 9503 (2015).
36. M. Ma, L. Guo, D. Anderson, R. Langer, Bio-inspired polymer composite actuator and generator driven by water gradients. *Science* **339**, 186–189 (2013).

Acknowledgments: We are indebted to Y. Rui and G. Wang for performing SEM and XPS analysis of the samples. **Funding:** We gratefully acknowledge the financial support by the NSF of China (no. 51172042), the Ministry of Education of China (IRT1221, no. 111-2-04), the Science and Technology Commission of Shanghai (13JC1400200 and 15ZR1401200), a Specialized Research Fund for the Doctoral Program of Higher Education (20110075130001), the China Postdoctoral Science Foundation, Eastern Scholar, and the Fundamental Research Funds for the Central Universities (2232014A3-06). **Author contributions:** J.M. and C.H. performed the experiments. J.M., C.H., and H.W. conceived and designed the experiments. M.Z., Q.Z., and Y.L. analyzed the data. J.M. and H.W. wrote the manuscript. All authors read and approved the final manuscript. **Competing interests:** The authors declare that they have no competing interests. **Data and materials availability:** All data needed to evaluate the conclusions in the paper are present in the paper and/or the Supplementary Materials. Additional data related to this paper may be requested from H.W. (wanghz@dhu.edu.cn) or Q.Z. (zhangqh@dhu.edu.cn).

Submitted 29 April 2015
Accepted 3 September 2015
Published 6 November 2015
10.1126/sciadv.1500533

Citation: J. Mu, C. Hou, H. Wang, Y. Li, Q. Zhang, M. Zhu, Origami-inspired active graphene-based paper for programmable instant self-folding walking devices. *Sci. Adv.* **1**, e1500533 (2015).